AN EDGE-PRESERVING STABILIZATION FOR A FAST 3-D IMAGING ALGORITHM WITH A UWB PULSE RADAR

Takuya Sakamoto[1], Shouhei Kidera[1], Toru Sato[1], and Satoshi Sugino[2]

[1]*Kyoto University, 606-8501 Sakyo-ku Yoshida-Honmachi, Japan*
[2]*New Product Technologies Development Department, Matsushita Electric Works, Ltd., 1048, Kadoma, Osaka 571-8686, Japan*

ABSTRACT

It is hoped that rescue robots help human lives in the near future. Recently, UWB(Ultra Wide Band) has been standardized in the USA, and it enables us to develop pulse radars with high range resolution. This technology is a promising candidate for the environment measurement for robots. Radar imaging is known as one of ill-posed inverse problems, for which various algorithms have been proposed. Most of them were developed for continuously distributed media such as the ground. Their calculation time is too long because they are based on iterative methods, which is not acceptable for the realtime operation of robots. On the other hand, most of in-house objects have clear boundaries, which enables us to simplify the models. We have already proposed a fast imaging algorithm SEABED for UWB pulse radars, which is based on a reversible transform by utilizing this simple model. The performance of the SEABED algorithms has been investigated only with numerical simulations. In this paper, we experimentally study the performance of the algorithm with a UWB pulse radar experiment system.

Key words: UWB (Ultra Wide-Band); radar imaging; inverse scattering.

1. INTRODUCTION

Radar imaging is an important technique which has a variety of applications including rescue robots for disaster areas. It is known that radar imaging is one of ill-posed inverse problems. A large number of algorithms have already been proposed for this problem [1, 2, 3, 4, 5, 6, 7, 8]. However, the conventional algorithms require long calculation time because they were developed for the imaging of general targets including continuously distributed media such as the inside of the ground or a human body. This problem causes a critical difficulty in applying radars to realtime operation which is needed for robots. In order to solve this problem, we have proposed a fast 3-dimensional imaging algorithm, SEABED [9, 10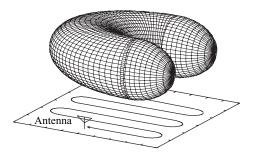, 11, 12, 13, 14]. This algorithm is based on a reversible transform between target shapes and observed signals under a certain condition. It has already been clarified that SEABED algorithm can accurately estimate 3-D target shapes in a short time with numerical simulations. However, the performance of SEABED algorithm has not been checked by experiments. In this paper, we apply SEABED algorithm to experimental data and investigate the performance of the algorithm. Additionally, we propose a smoothing algorithm which enable us to enhance the robustness of SEABED algorithm against a noisy environment. We apply this stabilization method to the experimental data, and show the results.

2. SYSTEM MODEL

We assume a mono-static radar system. An omni-directional antenna is scanned on a plane. UWB pulses are transmitted at a fixed interval and received by the antenna. The received data is A/D converted and stored in a memory. We estimate target shapes using the obtained data. Fig. 1 shows the system model.

We deal with a 3-dimensional problem. We define a real space, where targets and the antenna are located. We express the real space with the parameter (x, y, z). All of x, y and z are normalized by λ, which is the center wavelength of the transmitted pulse in the air. We assume $z > 0$ for simplicity. The antenna is scanned on x-y plane.

We define $s'(X, Y, Z)$ as the received electric field at the antenna location $(x, y, z) = (X, Y, 0)$, where we define Z with time t and speed of the radiowave c as $Z = ct/(2\lambda)$. We apply a matched filter of the transmitted waveform to the received signals $s'(X, Y, Z)$. We define $s(X, Y, Z)$ as the output of the filter. We normalize X and Y by λ, and Z by the center period of transmitted waveform, respectively. We define a data space expressed by (X, Y, Z). SEABED algorithm extracts quasi wavefronts which are equiphase-surfaces in the data space. The transform from the data space to the real space corresponds to imaging which we deal with in this paper.

Figure 1. The coordinates and an example of a target complex permittivity.

3. SEABED ALGORITHM

The following equations hold for (x, y, z) and (X, Y, Z).

$$\begin{cases} x & = & X - Z\partial Z/\partial X \\ y & = & Y - Z\partial Z/\partial Y \\ z & = & Z\sqrt{1 - (\partial Z/\partial X)^2 - (\partial Z/\partial Y)^2}, \end{cases} \quad (1)$$

This equation is called Inverse Boundary Scattering Transform (IBST). SEABED algorithm obtains the target shapes by calculating the right hand side of Eq. (1). Fig. 10 shows the estimated target shape in a numerical simulation. Here we assume the true target shape as in Fig. 1.

We have already developed a fast radar imaging algorithm based on BST (Boundary Scattering Transform) [9, 13]. We call the algorithm SEABED (Shape Estimation Algorithm based on BST and Extraction of Directly scattered waves). The algorithm utilizes the existence of a reversible transform BST between target shapes and pulse delays. We have clarified that the SEABED has an advantage of direct estimation of target boundaries using inverse transform, which is a mathematically complete solution for the inverse problem. The algorithm has a remarkable performance in estimating target shapes. The SEABED utilizes the existence of a reversible transform between quasi wavefronts and target boundary surfaces. We assume that each target has a uniform complex permittivity, and surrounded by a smooth boundary. We also assume that the propagation speed is known. Here, we assume the medium of direct path is vacuum for simplicity.

4. SYSTEM MODEL AND SEABED ALGORITHM

We assume a mono-static radar system in this paper. An omni-directional UWB antenna is scanned on a plane. We express the surface of the target in the real space with the parameter (x, y, z). These parameters are normalized by the center wavelength λ. $s(X, Y, Z)$ is the received signal at the antenna location $(x, y, z) = (X, Y, 0)$,
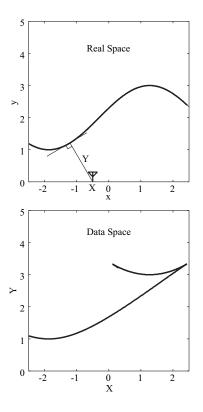

Figure 2. An example of a target shape and a quasi wavefront for 2-D systems.

where we define Z with time t and speed of the radiowave c as $Z = ct/(2\lambda)$. We define a quasi-wavefront $Z(X, Y)$ which is a equi-phase surface extracted from $s(X, Y, Z)$. SEABED algorithm is based on a reversible transform IBST. IBST describes the target shape (x, y, z) with the quasi-wavefront (X, Y, Z) as

$$\begin{cases} x & = & X - Z\partial Z/\partial X \\ y & = & Y - Z\partial Z/\partial Y \\ z & = & Z\sqrt{1 - (\partial Z/\partial X)^2 - (\partial Z/\partial Y)^2}. \end{cases} \quad (2)$$

5. CHARACTERISTICS OF QUASI-WAVEFRONTS

5.1. The Upper-bound for the Hesse Matrix of Quasi-Wavefronts

Smoothing is an effective tool to solve the problem that the image of the SEABED algorithm degrades due to random components caused by noise and timing jitter. For stationary signals, it is the best scheme to apply the smoothing by the convolution with the impulse response, which corresponds to the matched filter. However, target shapes as 2-D signals are not stationary because they have arbitrary shapes including planes, curved surfaces and edges, which implies that the smoothing is difficult to apply to them. On the other hand, the smoothing of

quasi-wavefronts is suitable for the stabilization without spoiling the resolution, because the quasi-wavefronts for convex targets are guaranteed to be smooth. The quasi-wavefronts, however, are neither stationary signal, so it is effective to adaptively change the kernel function to use for the smoothing depending on the smoothness of the surfaces. In this section, we deal with a Hesse matrix as a local smoothness of the surface of quasi-wavefronts, and discuss the Hesse matrix H_Z of the quasi-wavefront for concave targets. Additionally, we analytically derive the optimum smoothing method based on the characteristics of the quasi-wavefronts.

First, we investigate the characteristics of the Hesse matrix of concave surfaces. The Hesse matrix H_z for concave surface $z(x, y)$ is defined as

$$H_z = \left[\begin{array}{cc} z_{xx} & z_{xy} \\ z_{yx} & z_{yy} \end{array} \right], \qquad (3)$$

which is a positive definite matrix. Therefore, the following inequalities holds.

$$\mathrm{tr} H_z = z_{xx} + z_{yy} > 0 \qquad (4)$$
$$\det H_z = z_{xx} z_{yy} - z_{xy}^2 > 0 \qquad (5)$$

Next, we show that the inequality $x_X > 0$ holds, which characterize the position of the scattering center for convex targets. This inequality means that the scattering center for the received echo moves to the same direction as the antenna moves. This characteristic is important to investigate the Hesse matrix of a quasi-wavefront. By solving Eq. (2) for x and obtain

$$x = X - z z_x. \qquad (6)$$

We partially differentiate this equation for X with Y fixed and obtain

$$x_X = 1 - (z_x^2 + z z_{xx}) x_X - (z_x z_y + z z_{xy}) y_X. \qquad (7)$$

We solve this equation for x_X and obtain

$$x_X = \frac{1 - (z_x z_y + z z_{xy}) y_X}{1 + z_x^2 + z z_{xx}}. \qquad (8)$$

Similarly, we obtain y_X as

$$y_X = -\frac{(z_x z_y + z z_{xy}) x_X}{1 + z_y^2 + z z_{yy}}. \qquad (9)$$

By utilizing Eqs. (8) and (9), x_X is expressed as

$$x_X = \frac{1}{d_1 + d_2 + d_3 + d_4}, \qquad (10)$$
$$d_1 = 1 + z_x^2 + z_y^2, \qquad (11)$$
$$d_2 = z(z_{xx} + z_{yy}) = z\, \mathrm{tr} H_z, \qquad (12)$$
$$d_3 = z^2(z_{xx} z_{yy} - z_{xy}^2) = z^2 \det H_z, \qquad (13)$$
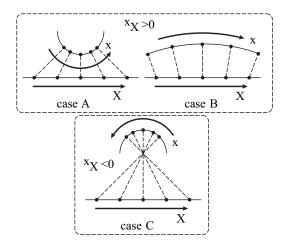$$d_4 = z(z_x^2 z_{yy} + z_y^2 z_{xx} - 2 z_x z_y z_{xy}), \qquad (14)$$

Figure 3. The relationship between the target shape and the sign of x_X for the 2-D case.

where $d_1 > 0$, $d_2 > 0$ and $d_3 > 0$ hold by utilizing $z > 0$ and Eqs. (4) and (5).

As for d_4, we discuss as follows. The discriminant of the 2nd order equation $d_4 = 0$ for z_x is $D = -4z^2 z_y^2 \mathrm{tr} H_z \leq 0$, $z^2 z_{yy}^2 > 0$ holds for the coefficient of z_x^2. Therefore, d_4 is the convex parabola smaller than 0, that means $d_4 \geq 0$. By considering the conditions for d_1, d_2, d_3, d_4, and Eq. (10),

$$x_X > 0 \qquad (15)$$

holds. Fig. 3 shows the relationship between the target shape and the sign of x_X for the 2-D system. In this figure, the antenna X and and the scattering center x move to the same directions for the cases A and B. On the other hand, they move to the opposite directions for the case C. The convex target dealt with in this paper corresponds to the case A. Note that these figures are for the 2-D system, not for the 3-D system, and the motion of the scattering center for the 3-D case also depends on the shape for the direction y, which is not so simple as the 2-D case in Fig. 3.

For point targets and edges, all of d_1, d_2, d_3 and d_4 in Eq. (10) diverge to $+\infty$ and the equation $x_X = 0$ holds. This means that the scattering center does not move because the echoes for point targets and edges are not reflections but diffractions. On the other hand, $x_X > 0$ always holds for smooth surfaces.

We investigate the upper-bound of the eigenvalues of the Hesse matrix H_Z for a quasi-wavefront by utilizing Eq. (15). With the upper-bound of the eigenvalues, we can estimate the smoothness of the quasi-wavefront obtained with the received data, which enables us to suitably select the correlation length for smoothing. We solve Eq. (2) for Z_X and obtain

$$Z_X = (X - x)/Z. \qquad (16)$$

We differentiate Eq. (16) for X and obtain

$$Z_{XX} = \frac{(1 - x_X)Z - (X - x)Z_X}{Z^2}. \qquad (17)$$

By substituting Eq. (16) to Eq. (17) and obtain

$$Z_{XX} = \frac{1 - Z_X^2 - x_X}{Z}. \qquad (18)$$

Because $x_X > 0$ in Eq. (15) holds, We obtain the following inequality

$$Z_{XX} < \frac{1 - Z_X^2}{Z}. \qquad (19)$$

This equation means that the diagonal elements of the Hesse matrix H_Z have the upper-bound, which is determined by the quasi-wavefront and its partial derivatives.

The smoothness of the curved surfaces is determined by the eigenvalues of the Hesse matrix. Especially, it is indispensable to know the maximum eigenvalue to suppress the distortion caused by the smoothing. Eq. (19) is one of the diagonal elements of the Hesse matrix. If X is parallel to the maximum eigenvector of the Hesse matrix at (X, Y), the right-hand side of the equation is the upper-bound of the maximum eigenvalue. Therefore, for the maximum eigenvalue e of the Hesse matrix H_Z,

$$e < \frac{1 - Z_V^2}{Z} \qquad (20)$$

holds, where Z_V is the partial derivative in the direction of the eigenvector for the maximum eigenvalue. Additionally, the following inequality holds because of $Z_V^2 \geq 0$ as

$$e < \frac{1}{Z}. \qquad (21)$$

This equation means that the upper-bound of the smoothness of the quasi-wavefront depends only on the time delay of the echo. The smoothness is guaranteed especially for the convex target in the far-field. The inequality of Eq. (21) becomes an equation for point targets or edges. The quasi-wavefronts for the point target on the z-axis, is expressed as hyperbolic surfaces $Z = \sqrt{X^2 + Y^2 + Z_0^2}$ for the distance Z_0 between the target and the scan plane. The vertical section on X-Z plane is shown in Fig. 4. This figure includes multiple quasi-wavefronts for different positions of point targets. The intercept of each curve is equal to the position Z_0.

This figure shows that the upper-bound of the curvature becomes small as the distance Z becomes large. Especially, the quasi-wavefront for the point target close to the scan plane has a large curvature around $X = 0$, which makes it difficult to smooth with long correlation length.

5.2. Proposed Smoothing Method

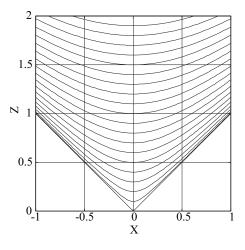In this section, we propose the smoothing method based on the discussion in the previous section. We deal with

Figure 4. Quasi wavefronts of the echoes from point targets.

the smoothing by the convolution with a Gaussian function

$$g(X, Y; \sigma) = \frac{1}{2\pi\sigma^2} \exp\left(-\frac{X^2 + Y^2}{2\sigma^2}\right). \qquad (22)$$

This Gaussian function includes only one parameter σ, the correlation length. We adaptively change σ depending on the smoothness of the quasi-wavefront. For example, if the eigenvalue of the Hesse matrix of the quasi-wavefront is small, the quasi-wavefront is close to a plane, to which we can apply the smoothing with a long correlation length. On the contrary, we have to set short correlation length for large eigenvalues in order to avoid the degradation of the resolution of the image. If we know the Hesse matrix H_Z, we can obtain the suitable parameter of the Gaussian function by utilizing the eigenvector. However, it is needed to calculate the 2nd derivative in order to obtain the Hesse matrix, which can be the cause of the instability. In our proposed method, we utilize the Eq. (21) instead of the calculation of the Hesse matrix. The right-hand side of Eq. (21) overestimate the curvature of the quasi-wavefront, which means that we can avoid the degradation of the resolution.

We determine the correlation length as follows. We define the distortion δ caused by the smoothing with a Gaussian function as

$$\delta = \left| \int \int_{-\infty}^{\infty} g(X, Y; \sigma)Z(X, Y)\mathrm{d}X\mathrm{d}Y - Z(0, 0) \right|. \qquad (23)$$

We locally replace the quasi-wavefront by the quadratic surface $Z(X, Y) = a(X^2 + Y^2)/2 + bX + cY + d$ at $(X, Y) = (0, 0)$. For the quadratic surface, the characteristic equation has a double root, and the maximum eigenvalue is $e = a$. We estimate the worst distortion by utilizing the quadratic surface. The maximum correlation length σ for a certain acceptable distortion $\delta_{\max}$ is determined as $\sigma \leq \sqrt{\delta_{\max}/\pi a}$ by utilizing Eq. (23). Considering the condition $a = e < 1/Z$ based on Eq. (21), we
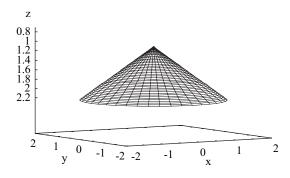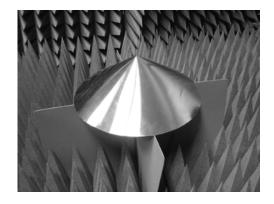
Figure 5. True target shape.

Figure 6. Conical metallic object used for the experiment.

Figure 7. Quasi wavefront extracted from the experimental data.

Figure 8. Estimated target shape of SEABED algorithm without smoothing.

obtain

$$\sigma = \sqrt{\delta_{\max} Z / \pi}. \tag{24}$$

We propose the smoothing by the convolution with the Gaussian function with the correlation length the right-hand side of Eq. (24).

6. EVALUATION OF THE PROPOSED SMOOTHING BY AN EXPERIMENT

In this section, we apply the SEABED algorithm to the experimental data, and investigate the performance of the proposed algorithm. We deal with 3 types of smoothing, the one without smoothing, the one with the smoothing in the real space, and the one with the proposed smoothing in the data space.

The target shape used for an application example is the conical metallic object shown in Fig. 5. For the center wavelength 9.1cm, the radius of the bottom is $1.64\lambda(14.9\text{cm})$, the height is $1.1\lambda(9.8\text{cm})$, the distance between the vertex and the scan plane is $0.93\lambda(8.5\text{cm})$. The cone is a difficult to smooth because it includes both of a smooth surface and a sharp edge. The target object used in our experiment is shown in Fig. 6.

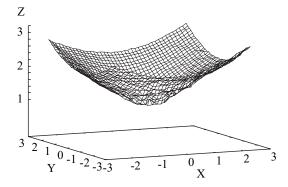We investigate the performance of the SEABED algorithm for experimental data. Fig. 7 shows the quasi-

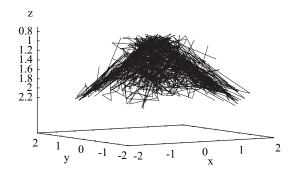wavefront estimated with the experimental data. We see random component with large error around the center of the quasi-wavefront because the echo around the center is not a reflection but a diffraction, which has relatively small S/N. Fig. 8 shows the estimated image obtained by the original SEABED algorithm without smoothing, where we utilize the modified transform to compensate for the distance between the antennas [15]. The experimental data contain random components such as noise and timing jitter. The inverse transform utilize the derivative operations, which is sensitive the random components. Fig. 9 shows the smoothed image obtained by applying the smoothing with the correlation length of 0.1λ to the image in Fig. 8. The quality of this image is poor both for the resolution and the stability against noise.

Next, we apply the proposed smoothing method to the experimental data. Fig. 10 shows the estimated image by utilizing the proposed smoothing technique with the suitable correlation length σ determined in Eq. (24). Here we empirically set the acceptable distortion as $\delta_{\max} = 0.12\lambda$. In this figure, the smooth surface and edge are correctly estimated, which means that both of the resolution and stability are achieved by the proposed method. Especially, the proposed algorithm preserves the edge while the random components are suppressed well.
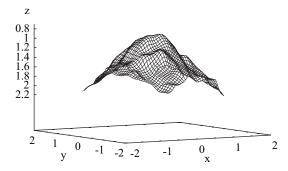
Figure 9. Estimated target shape of SEABED algorithm with a smoothing in the real space.
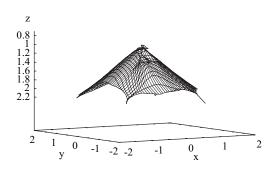

Figure 10. Estimated target shape of SEABED algorithm with the proposed smoothing in the data space.

REFERENCES

1. E. J. Bond, X. Li, S. C. Hagness, and B. D. van Veen, "Microwave imaging via space-time beamforming for early detection of breast cancer," IEEE Trans. Antennas Propagat., vol. 51, no. 8, pp. 1690–1705, 2003.

2. R. M. Narayanan, X. Xu, and J. A. Henning, "Radar penetration imaging using ultra-wideband (UWB) random noise waveforms," IEE Proc.-Radar Sonar Navig., vol. 151, no. 3, pp. 143–148, 2004.

3. J. van der Kruk, C. P. A. Wapenaar, J. T. Fokkema, and P. M. van den Berg, "Three-dimensional imaging of multicomponent ground-penetrating radar data," Geophysics, vol. 68, no. 4, pp. 1241–1254, 2003.

4. C. J. Leuschen and R. G. Plumb, "A matched-filter-based reverse-time migration algorithm for grond-penetrating radar data," IEEE Trans. Geoscience & Remote Sensing, vol. 39, no. 5, pp. 929–936, May 2001.

5. T. J. Cui, Y. Qin, G. L. Wang, and W. C. Chew, "High-order inversion formulas for low-frequency imaging of 2D buried targets," Proceedings of 2004 IEEE Antennas and Propagation Society International Symposium, vol. 1, pp. 189–192, 2004.

6. W. C. Chew and Y. M. Wang, "Reconstruction of two dimensional permittivity distribution using the distorted Born iterative method," IEEE Trans. Med. Imaging, vol. 9, no. 2, pp. 218–225, 1990.

7. P. Lobel, C. Pichot, L. Blanc-Feraud, and M. Barlaud, "Microwave imaging: Reconstructions from experimental data using conjugate gradient and enhancement by edge-preserving regularization," International Journal of Imaging Systems and Technology, vol. 8, no. 4, pp. 337–342, Dec. 1998.

8. T. Sato, T. Wakayama, and K. Takemura, "An imaging algorithm of objects embedded in a lossy dispersive medium for subsurface radar data processing," IEEE Trans. Geosci. Remote Sensing, vol. 38, no. 1, pp. 296–303, 2000.

9. T. Sakamoto and T. Sato, "A target shape estimation algorithm for pulse radar systems based on boundary scattering transform," IEICE Trans. Commun., Vol. E87-B, No. 5, pp. 1357–1365, May, 2004.

10. T. Sakamoto and T. Sato, "Fast imaging of a target in inhomogeneous media for pulse radar systems," Proc. 2004 IEEE International Geoscience and Remote Sensing Symposium Vol. 3, pp. 2070–2073, Sep. 2004.

11. T. Sakamoto and T. Sato, "A phase compensation algorithm for high-resolution pulse radar systems," IEICE Trans. Communications, vol. E87–B, no. 11, pp. 3314–3321, Nov., 2004.

12. T. Sakamoto and T. Sato, "A phase compensation algorithm for high-resolution pulse radar systems," Proc. 2004 International Symposium on Antennas and Propagation, pp. 585–588, Aug. 2004.

13. T. Sakamoto and T. Sato, "A fast algorithm of 3-dimensional imaging for pulse radar systems," Proc. 2004 IEEE AP-S International Symposium and USNC/URSI National Radio Science Meeting, vol. 2, pp. 2099–2102, June, 2004.

14. T. Sakamoto, S. Kidera, T. Sato, T. Mitani and S. Sugino, "An experimental study on a fast imaging algorithm for UWB pulse radar systems," Proc. 2005 IEEE AP-S International Symposium and USNC/URSI National Radio Science Meeting, July, 2005.

15. S. Kidera, T. Sakamoto, and T. Sato, "A high-resolution 3-D imaging algorithm with linear array antennas for UWB pulse radar systems," IEEE AP-S International Symposium, USNC/URSI National Radio Science Meeting, AMEREM Meeting, July, 2006.